Green Chemistry

Accepted Manuscript

ROYAL SOCIETY OF CHEMISTRY

www.rsc.org/greenchem

Journal Name

ARTICLE

Evaluation of transition metal phosphides supported on ordered mesoporous materials as catalysts for phenol hydrodeoxygenation

Received 00th January 20xx,
Accepted 00th January 20xx

DOI: 10.1039/x0xx00000x

www.rsc.org/

A. Berenguer[a], T. M. Sankaranarayanan[a], G. Gómez[b], I. Moreno[a,b], J. M. Coronado[a], P. Pizarro[a,b], D. P. Serrano*[a,b]

A series of transition metal phosphides (Ni_2P, Co_2P and MoP) have been synthesized by temperature programmed reduction of the corresponding metal phosphate precursors loaded over mesostructured Al-SBA-15, mesoporous ɣ-Al_2O_3 (m-Al_2O_3) and ordered mesoporous carbon (CMK-3). Both the dispersion and metal phosphide phases attained are strongly influenced by the support features, such as its acidic and textural properties. XRD, TEM and H_2 chemisorption results revealed that MoP phase was probably formed but it undergoes a fast re-oxidation in air. On the other hand, metal phosphide formation was hindered over m-Al_2O_3 as only metallic Ni and Co were detected. All the materials prepared have been evaluated as catalysts in hydrodeoxygenation (HDO) using phenol as bio-oil model compound. The highest phenol conversions were attained with the catalysts based on the acidic supports (Al-SBA-15 and m-Al_2O_3). Nevertheless, Co_2P/Al-SBA-15, Ni_2P/m-Al_2O_3 and Co_2P/m-Al_2O_3 yielded cyclohexanol as main product denoting very low HDO efficiency. In contrast, Ni_2P/Al-SBA-15 showed remarkable catalytic properties, being the only catalyst providing almost full phenol conversion and extremely high HDO efficiency, with cyclohexane selectivity higher than 90 %. This may be due to a synergetic effect between the high electron deficiency, generated by the $Ni^{\alpha+}$ ($0 < \alpha < 1$) species owing to an electron transfer from Ni to P, and the different acid sites present in the catalyst.

Introduction

On account of the elevated consumption of non-renewable fossil fuels and the huge CO_2 emissions associated with the transport sector, the exploitation of renewable energy resources has increased its importance significantly around the world. Accordingly, the European Union has set a target of 10% from renewable sources for energy of the transportation sector by the year 2020. Fuels derived from biomass, so-called biofuels, could play an important role as substitutes of petroleum-based fuels currently used. In particular, lignocellulosic biomass has attracted great attention as raw material because it is very abundant and does not compete with food industry.[1] Lignocellulose, which is responsible of the structural stability in the plant cell walls, is composed of two carbohydrate polymers (cellulose and hemicellulose) and one aromatic polymer formed by phenolic molecules (lignin). Thermochemical treatments of lignocellulosic biomass, such as pyrolysis, gasification and liquefaction are used to obtain bio-oils which will be later converted into liquid bio-fuels.[2] Among them, fast pyrolysis maximizes the production of bio-oil but, unfortunately, this liquid fraction presents too high content of oxygenates (organic acids, aldehydes, ketones, sugars, aromatics, etc.) leading to relatively low calorific value. Likewise there are other poor properties, including high viscosity, corrosiveness, immiscibility with hydrocarbon fuels, etc., which hinders the direct use of pyrolysis bio-oil in vehicle engines.[3] Accordingly, it is necessary to apply additional downstream upgrading treatments in order to produce real substitutes to conventional fuels from pyrolysis of lignocellulosic biomass.[4,5] In this sense, one of the most promising upgrading routes is the catalytic hydrodeoxygenation (HDO) reaction. This procedure consists on subjecting the bio-oil to moderate temperatures (250-450 °C) and high hydrogen pressure (20-300 bar) in the presence of heterogeneous catalysts, so that the oxygen contained in organic compounds is removed in the form of water without unnecessary loss of carbon and, ideally, without undesired hydrogen consumption.[6,7]

The investigation in this field started in the 1980's and the first catalytic systems explored were those used at industrial scale in hydrodesulphurization (HDS) processes, such as Co-MoS_2 and Ni-MoS_2 supported on alumina.[7–10] In those systems, the sulphur anion vacancies or the coordinatively unsaturated sites (CUS) located at the edges of MoS_2 slabs have been often proposed as the active sites for both HDS and HDO. However, because of the substitution of sulphur by oxygen atoms as the reaction progresses, deactivation of the sulphide catalysts occurs. In order to maintain the stability and activity of these

[a] IMDEA Energy Institute, Avda. Ramón de la Sagra 3, Parque tecnológico de Móstoles, 28935, Móstoles, Madrid, Spain.
[b] Chemical and Environmental Engineering Group, ESCET, Universidad Rey Juan Carlos, C/ Tulipán SN, 28933, Móstoles, Madrid.

catalysts, it is necessary the addition of sulphur-containing compounds (e.g., H_2S and CS_2) which react and preserve the catalyst sulfurization. Nevertheless, the use of these reagents leads to sulphur pollution of the final products.[11–13] Furthermore, the existence of acid sites on the alumina surface favours the deactivation by coke deposition. As an attempt to avoid this last problem, active carbons have been proposed as supports, leading to a major selectivity towards deoxygenated products but with lower conversions.[14] Another option to prevent coke formation is supporting MoS_2 over less acidic metal oxides, such as zirconia and titania. It has been found that these materials not only reduce the coke deposition but also they favour the formation of small MoS_2 crystallites leading to a better dispersion of the active phase.[15,16]

Noble metal catalysts, such as Ru, Pd, Pt, etc., have been also studied for the HDO process.[17] These materials have shown to be active at lower temperatures and, therefore, they could be able to inhibit secondary thermal reactions which lead to an operational instability, aside from coke formation and deactivation. In addition, these catalysts can be supported over materials with good hydrothermal stability, such as carbons, zeolites and SBA-15.[18,19] Depending on the catalyst design, both conversion and deoxygenation degree were even higher than in the case of traditional sulphide catalysts. Nevertheless, noble metal catalysts are expensive and they need large hydrogen consumption to obtain high selectivity for hydrogenation reactions. Additionally, these catalysts show low resistance towards the poisoning caused by small amounts of sulphur compounds.[20]

As alternatives to the unstable sulphides and the expensive noble metal catalysts, metal carbides and nitrides have been proposed for hydrogenation reactions, in particular molybdenum nitrides and carbides due to their good hydrogen transfer properties.[21,22] Transition metal oxides have been also investigated in the hydroprocessing field. Metal oxidized catalysts can be reduced producing anionic vacancies, which create surface defects suitable to catalyze hydrogenolysis and hydrogenation reaction at typical HDO conditions.[23–25]

In the last years, transition metal phosphides have been studied as a new type of catalysts. The physicochemical properties of metal-rich phosphides (MP and M_2P) are similar to those of ceramic compounds such as carbides, nitrides, borides and silicides. These materials combine properties of ceramics and metals, being remarkable their excellent heat and electric conductivity, as well as high thermal and chemical stability. Nevertheless, their crystal structure is essentially different than in carbides and nitrides.[26] Numerous research articles have stated the excellent properties in the hydrotreating process of transition metal phosphides, especially for HDS and HDN of petroleum feedstocks. Chen et al. have reported that deoxygenation of methyl laurate is higher using Ni_2P phase synthesized with a molar ratio of Ni/P lower than the stoichiometric one.[27] Likewise, Koranyi et al. have concluded that it is necessary to introduce an excess of phosphorous in order to achieve the formation of the most active phase Ni_2P.[28] The presence of phosphorus plays an important role in Ni_2P activity. Firstly, P sites produce a "ligand" effect on the metal sites altering the electron density of the metal cation, which facilitates the hydrogen dissociation. Additionally, Ni_2P phase may have P–OH groups associated with moderate acidity which favours the hydrogenation reactions.[29,30] In addition, several studies have reported that supported transition metal phosphides such as Ni_2P/SiO_2, Fe_2P/SiO_2, MoP/SiO_2, Co_2P/SiO_2 and WP/SiO_2 lead to high conversions in HDO of typical model compounds of bio-oils such as phenol[31], guaiacol[32], furan[33] and anisole.[34]

The method usually followed to prepare transition metal phosphides (both bulk and supported) is by temperature-programmed reduction (TPR) of the corresponding metal phosphates.[35] This reduction is carried out at high temperatures according to the high strength of the P-O bond.[36] However, these severe conditions can reduce the surface area and, therefore, the catalytic activity of the catalysts. Consequently, several studies have explored the use of porous supports in order to enhance the dispersion of the metal phosphides and hinder their sinterization.[37]

In this context, the aim of the current work is to report our results concerning the dispersion and catalytic activity evaluation in HDO reaction of three transition metal phosphides (Ni_2P, Co_2P and MoP) over three types of mesoporous supports with different textural, physicochemical and acidic properties: mesostructured Al-SBA-15, ordered mesoporous high surface area carbon CMK-3 and mesoporous ɣ-alumina (m-Al_2O_3). The catalysts have been characterized by adsorption-desorption of N_2 (77 K), XRD, TEM, ICP-OES, NH_3-TPD and H_2-TPR techniques in order to establish the correlation between the catalyst properties and their HDO activity.

The catalytic reactions have been carried out using phenol as model substrate because phenolic compounds represent approximately 25% of oxygenates present in pyrolysis bio-oils, while they have shown low reactivity in HDO treatments[38], and therefore, its study could provide important information for improving the upgrading process of pyrolysis oils.

Experimental

Catalysts preparation

Synthesis of Al-SBA-15. Al-SBA-15 mesoporous material was synthesized according to the procedure described elsewhere.[39] In a typical synthesis, 17 g of silica source, tetraethylorthosilicate (TEOS, Aldrich), and 0.249 g of aluminium isopropoxide (AIP, Aldrich) as Al source [$(Si/Al)_{MOL}$=67] were added to 20 ml of an aqueous HCl solution of pH 1.5. This mixture was stirred about 3 h until a homogenous solution was obtained. Then, this solution was added to a second one containing 8 g of a non-ionic triblock copolymer (Pluronic P123, Aldrich) solved in 300 ml of HCl at pH 1.5. The final mixture was stirred for 20 h at 40 °C and aged under static conditions and autogenous pressure at 110 °C for 24 h. The solid product obtained was filtered, dried overnight and calcined in static air at 550 °C for 5 h with a heating rate of 1.8 °C/min in order to remove the surfactant.

Synthesis of m-Al_2O_3. Mesoporous ɣ-alumina material was synthesized according to a sol-gel method described in literature.[40] In this method 7.9 g of aluminium isopropoxide were first dissolved in 40 g of isopropanol (Scharlau). Another solution was prepared by mixing 7.3 g of HCl (35% wt. Scharlau), 4.3 g of hexadecyltrimethylammonium bromide (Aldrich) and 10 ml of deionized water. After stirring roughly both solutions for 30 min, they were mixed and further stirred at room temperature for 4 h. Then the synthesis mixture was heated at 80 °C and the obtained gel was dried at 110 °C for 15 h. Finally, the material was calcined in static air in two steps: firstly, heating at 110 °C for 2 h with a heating rate of 10 °C/ min, and secondly, heating at 550 °C for 5 h using a heating ramp of 1.8 °C/ min.

Synthesis of CMK-3. Ordered mesoporous carbon (CMK-3) was synthesized using a nanocasting pathway with pure silica SBA-15 as hard template, following the procedure reported in literature.[41,42]

First, SBA-15 was prepared by a soft-templating route described elsewhere[43,44], employing tetraethylorthosilicate (TEOS, Aldrich) and Pluronic P123 as silica source and structure directing agent, respectively. Typically, 4 g of Pluronic P123 were dissolved in a mixture containing the following composition: 0.0041 mol TEOS: 6.67 mol H_2O: 0.024 mol HCl. Afterwards, the solution was subjected to hydrolysis-condensation reaction at 40 °C for 6 h and hydrothermal treatment at 90 °C during 3 days. Finally, the filtrated solids were calcined at 550 °C during 6 h under static air.

For the synthesis of CMK-3 carbon, furfuryl alcohol (FA, Acros Organics) was used as precursor and oxalic acid (OA, Acros Organics) as polymerization catalyst. The pores of SBA-15 were filled with a solution containing 0.012 g OA per 3 mL FA through the wetness impregnation technique. Subsequently, the carbon precursor was polymerized within the SBA-15 pores by heat treatment at 50 °C for 1 day, and later at 90 °C for 2 days. Then, carbonization was carried out under inert atmosphere with the following temperature program: a) heating up to 150 °C for 3 h; b) heating up to 300 °C at 1 °C/min; c) heating up to 850 °C at 5 °C/min and d) keeping the last temperature for 3 h. Finally, the silica template was removed by dissolution with an ethanol-water mixture containing 1 M NaOH. The black powders so obtained were then filtrated, washed and dried at 90 °C overnight. By thermogravimetric analysis it was confirmed the effective elimination of the silica template, whose concentration remained below 5 wt.%.

Metal phosphide precursors incorporation

Precursors of metal phosphides were loaded into the catalytic supports by wetness impregnation technique. Thus, 1 g of support was dispersed into 1 mL of an aqueous solution containing $(NH_4)_2HPO_4$ (Aldrich) and a metallic salt, $Ni(NO_3)_2{\cdot}6H_2O$ (Aldrich), $Co(NO_3)_2{\cdot}6H_2O$ (Aldrich) or $(NH_4)_6Mo_7O_{24}{\cdot}4H_2O$ (Aldrich), using a Me/P molar ratio of 1.0 and with a total metal phosphide loading of 10 wt.%. Afterwards, the samples were dried at room temperature overnight, then at 120 °C for 24 h and subsequently calcined at 500 °C for 4 h under static air conditions.

Catalysts characterization

Porous properties were measured by nitrogen adsorption-desorption experiments at 77 K on a Quadrasorb system (from Quantachrom). The surface area was calculated using the B.E.T. equation, and the total pore volume was determined at a relative pressure of 0.97. The Barrett-Joyner-Halenda (BJH) method was used to estimate the pore size distribution using the adsorption branch of the isotherm.

X-ray diffraction (XRD) patterns of the catalysts were recorded with a Philips PW 3040/00 X'Pert MPD/MRD diffractometer using Cu Kα radiation operated at 45 kV and 40 mA. Crystalline phases were identified by checking reflection signals appearing in the XRD patterns with JCPDS (Joint Committee on Powder Diffraction Standards) data files. The metal phosphide crystallite size was calculated by the Scherrer´s equation. A high-temperature chamber was used to check the formation of Mo phosphide under conditions similar to those employed in the reduction treatments. For these tests the sample was subjected to the following temperature program under hydrogen flow (80 ml/min): a) heating from room temperature up to 350 °C at a rate of 5 °C/min; b) heating from 350 °C to 600 °C at a rate of 1 °C/min, c) isothermal conditions during 3 h and d) cooling down in H_2. The highest temperature reached was 600 °C instead of 650 °C because of the limitations of the chamber employed.

Transmission electron microscope (TEM) images were obtained on a PHILIPS TECNAI 20T instrument, working at 200 kV and equipped with an EDX spectrometer for measuring X-ray energy dispersive spectra. The powder sample was ultrasonically dispersed in acetone and then deposited on a porous carbon film supported on a copper grid.

Metal and phosphorus contents were measured by a Varian VISTA-MPX Inductively Coupled Plasma-Optical Emission Spectrometer (ICP-OES).

The complete reducibility of the catalysts was checked by hydrogen temperature-programmed reduction (H_2-TPR) in a quartz U-tube reactor with 100 mg of sample loading in the thermostatic zone. The TPR profiles were obtained by passing a 10 vol % H_2/Ar flow (50 ml/min) through the sample while heating from room temperature to 1000 °C, with a heating rate of 10 °C/min. The hydrogen consumption was determined by calibration and further integration of the output signals of the thermal conductivity detector (TCD). A cooling trap (liquid N_2 and isopropanol) placed between the sample and the TCD was used to retain the water produced during the reduction test.

The acidity of materials was measured by temperature programmed desorption of ammonia (NH_3-TPD) using the same setup as in the H_2-TPR measurements. The procedure followed for the TPD measurements involved the pre-treatment of the catalyst by flowing He at 600 °C for 1h, cooling to 100 °C, flowing a He/NH_3 mixture and removing the weakly physisorbed ammonia by passing helium at that temperature for 30 min. Thereafter, the chemisorbed

ammonia was desorbed by increasing the temperature up to 550 °C with a ramp of 10 °C/min, its concentration in the effluent stream being monitored by a TCD signal.

Catalytic activity measurements

The activity of the catalytic systems in phenol HDO was studied in a 100 ml stainless steel (SS) high-pressure stirred batch reactor. Firstly, 50 ml of a solution containing 3.5 wt.% phenol (Aldrich) in decalin (Aldrich), along with 0.1 g of catalyst was loaded into the reactor.

Prior to the reaction tests, calcined samples were pelletized, crushed and sieved with a 60-40 mesh (250-180 µm). Then, the metal phosphide phases were prepared by Temperature-Programmed Reduction (TPR) of the corresponding phosphate precursors[35] using a tubular furnace and the following temperature program under H_2 flow (80 ml/min): a) heating from room temperature up to 350 °C at a rate of 5 °C/min; b) from 350 °C to 650 °C at a rate of 1 °C/ min and c) isothermal conditions during 3 h. After the last reduction step, the sample was passivated by progressively introducing a stream of synthetic air at room temperature, as described in literature.[45] The reduction temperature was selected in order to preserve the support structure since at temperatures above 700°C the mesoporous structure of m-Al_2O_3 collapses. Likewise, in the case of ordered mesoporous carbon (CMK-3), the utilization of higher temperatures could promote losses of carbon by hydrogenation of the support.

Prior to start the reaction, once the autoclave reactor was closed, it was purged by flowing pure N_2 at room temperature. After that, the reactor was filled with 40 bar of pure H_2 and immediately heated up to the reaction temperature (220 °C) under vigorous stirring (1000 rpm). After 2 h of reaction, the autoclave was cooled down rapidly with cold water and ice. Reactant and products were analyzed off-line by gas chromatography (Agilent, 7890 A) equipped with a FID detector and a HP-INNOWAX column, as well as by GC-MS (Bruker, BP-5ms; 5% diphenyl/ 95% dimethyl polysiloxane column).

The catalytic activity of each material was evaluated in terms of phenol conversion, X_{PHE} *(%)*, and deoxygenation degree, *HDO (%)*. These parameters were calculated using the following equations:

$$HDO(\%) = \frac{n^0_{PHE} \times X_{PHE} - \sum_i n_i a_i}{n^0_{PHE} \times X_{PHE}} \times 100 = \left(1 - \frac{\sum_i n_i a_i}{n^0_{PHE} \times X_{PHE}}\right) \times 100 \quad (1)$$

$$X_{PHE}(\%) = \frac{n^0_{PHE} - n^F_{PHE}}{n^0_{PHE}} \times 100 \quad (2)$$

Where n^0_{PHE} is the initial amount of phenol (mol), n^F_{PHE} is the final amount of phenol (mol), n_i is the amount of i-product (mol) in the liquid phase (except for unreacted phenol) and a_i is the number of oxygen atoms in the molecule for each i-product.

Results and discussion

Physicochemical properties of the catalysts

Previously to the reaction tests, all samples were characterized by a series of techniques with the aim to correlate their physicochemical properties and metal phosphide-support interactions with the activity results.

Fig. 1 represents the N_2 adsorption-desorption isotherms at 77 K and the corresponding pore size distribution measured for all the supported materials in reduced form, in addition to the unloaded supports. In all cases type IV isotherms, typical of mesoporous materials, were obtained. For Al-SBA-15 based materials (Fig. 1a), the adsorption branch of the isotherms shows a narrow hysteresis loop in the P/P_0 region between 0.4-0.8 due to capillary condensation within the mesopores.[46] This loop exhibits two steps in the desorption branch denoting the presence of bottle-neck shaped pores.[47] As a general trend, loading all the supports with 10 wt.% of metal phosphides led to a severe decrease on the adsorbed volume but without modifying the isotherm shape. This reduction on the N_2 adsorption was accompanied by a decrease on the textural properties, as it can be seen in both BET surface area and total pore volume values presented in Table 1

In general, the degree of surface area loss was higher in catalysts based on both Al-SBA-15 and m-Al_2O_3, exhibiting surface areas between 40-60% lower than the original support, than that observed for the CMK-3 supported materials, which suffer a reduction close to 35%.

Regarding the pore size distribution (Fig. 1d, 1e and 1f), no significant changes were observed on the catalysts in comparison with the supports, except in the case of Al-SBA-15-based catalysts for which a slight reduction on the mean pore diameter were always observed. This pore diameter decrease suggests that some metal phosphides particles have been deposited along the mesopores that formed the Al-SBA-15 structure during the impregnation process.

The X-ray diffraction (XRD) patterns of both supports and reduced catalysts are shown in Fig. 2. The ordered mesoporous structure of Al-SBA-15 was evidenced at low angle (Fig. 2a), both before and after the incorporation of the different active phases. In the case of Al-SBA-15 support, three well defined peaks corresponding to (100), (110) and (200) reflections, representative of a 2D hexagonal pore system (*p6mm*) were clearly detected. However, after loading the metal phosphides, the last two reflections were imperceptible and the main diffraction signal (100) was slightly shifted towards higher angles. This result is in agreement with the drastic drop of the textural properties exhibited by these samples, and is a consequence of the very high metal phosphide dispersion levels achieved over this support together with partial blocking of the pores during the impregnation treatment. The ordered mesoporous carbon, CMK-3, exhibited the same three characteristic peaks at low angle, indicating that it has been

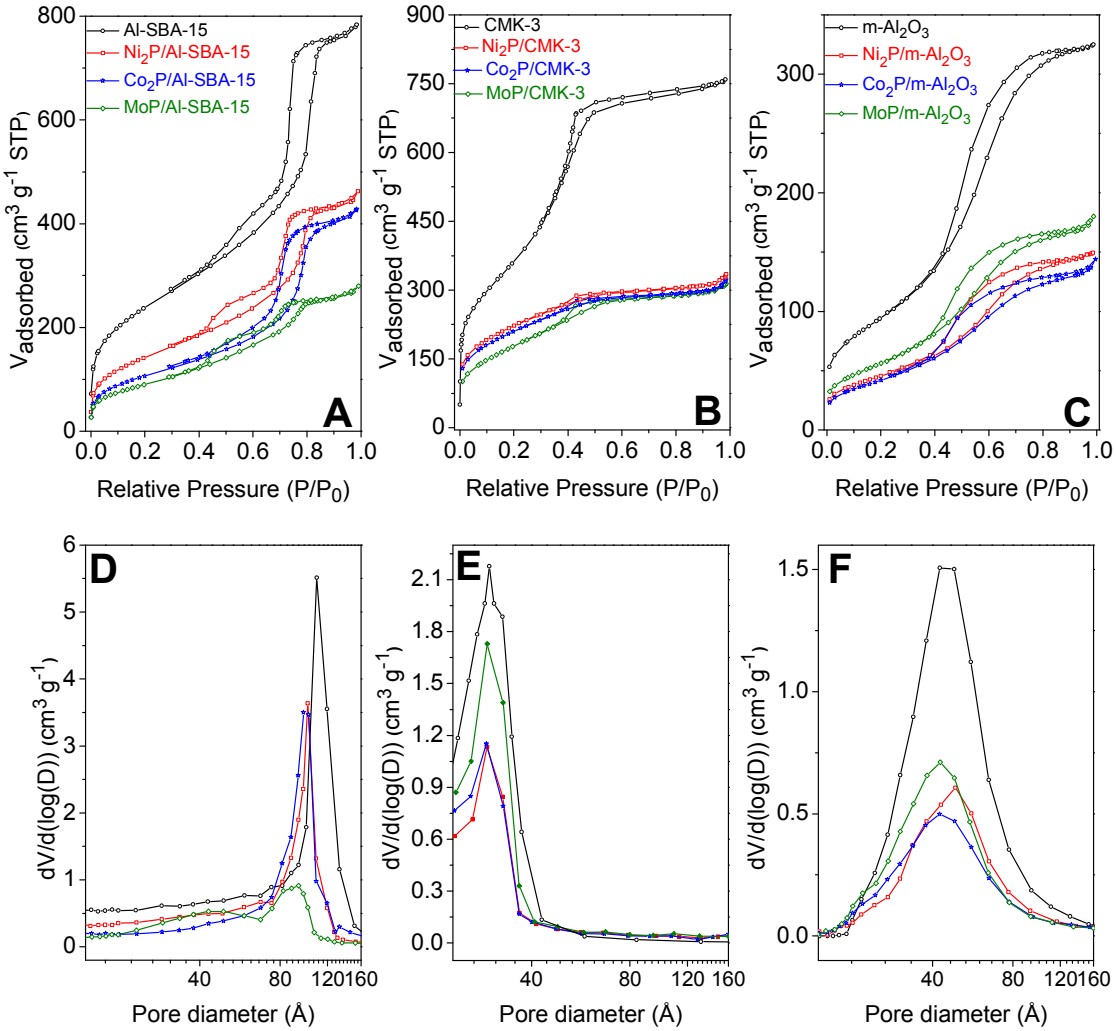

Fig 1 N_2 adsorption-desorption isotherms at 77 K (A, B and C) and pore size distribution employing BJH method (D, E and F) corresponding to both the supports and passivated supported catalysts.

successfully replicated the porous hexagonal symmetry of the hard template (SBA-15) used for its synthesis. Nevertheless, these peaks totally disappeared in the supported catalysts, denoting an apparent loss of mesoscopic order. In the case of mesoporous alumina, m-Al_2O_3, a broad diffraction signal appeared both in the support and supported catalysts, typical of non-ordered materials but having some homogeneity of both the pore size and wall thickness along the particles.

High angle XRD patterns were collected in all prepared materials in order to confirm the formation of metal phosphide phases after the reduction treatment. For Ni_2P and Co_2P over Al-SBA-15 and CMK-3 (Fig. 2b and 2d), reflections corresponding to such phosphide phases were evidenced, the first support leading to more intense signals indicative of higher crystallinity and crystal sizes. On the contrary, these metal phosphides were not observed over m-Al_2O_3 support while characteristic peaks corresponding to metallic Ni and Co species appeared (Fig. 2f). It is inferred that the establishment of different types of metal-support interactions promoted the preferential formation of Ni^0 and Co^0. Regarding the MoP phase, representative reflections were not detected in any sample, which can be attributed to either a very high dispersion of this phase, leading to extremely small nanoparticles, or to an incomplete reduction of the metal phosphide precursor.

Fig. 3 shows representative TEM images of all the catalysts prepared after the reduction and passivation treatment. It can be observed that the well-ordered hexagonal formation of cylindrical channels was kept after active phase incorporation into both mesostructured supports, Al-SBA-15 and CMK-3, (Fig. 3a-f), which is in agreement with the N_2 physisorption isotherms. The apparent partial or total loss of mesoscopic order in CMK-3 based samples, suggested by the low angle XRD patterns, is therefore attributed to the incorporation

process of the metal phosphides, leading to a large coverage of both the internal and external surface of the support. Both Ni_2P and Co_2P nanoparticles are always clearly distinguished, independently of the support employed. However, MoP particles were not observed in any case (Fig. 3c, 3f and 3i), in accordance with the high-angle XRD patterns, suggesting the formation of very well dispersed Mo species.

For Ni_2P and Co_2P supported catalysts, the distribution of particle sizes was estimated from TEM images and it is represented in Fig. 3, whereas the average size values are displayed in Table 1. These data show that the average size of the active phase is smaller than 10 nm for Ni_2P and 9.5 nm for Co_2P. In the case of ordered mesoporous carbon and m-Al_2O_3 catalysts, the mean diameter of the active phases is larger than the pore size, indicating than the majority of particles are located at the external surface, as confirmed by TEM (Fig. 3). Crystallite size values determined by the Scherrer's equation are shown in Table 1. In general, they are close to the mean size of metal phosphide particles measured from TEM micrographs, suggesting the particles of the active phase are monocrystalline. It is also remarkable a significant heterogeneity in the distribution of Ni and Co phosphide nanoparticles over Al-SBA-15, with significantly larger crystals over the external surface and others smaller and slightly elongated inside the channels (Fig. 3a and 3b). On the other hand, a more homogeneous particle distribution was observed over the CMK-3 carbon, this behaviour is especially more pronounced with Co_2P as active phase, for which the highest dispersion was achieved (Fig. 3d and 3e). In the case of m-Al_2O_3 support, the nanoparticles corresponding to the active phases, mainly in metallic form according to XRD results, exhibited a larger trend to form aggregates (Fig. 3g and 3h). In conclusion, the general dispersion of the metal derived phases over the supports increases in the following order: Al-SBA-15 < m-Al_2O_3 < CMK-3.

The chemical composition of all the catalysts was determined by ICP-OES analysis, the results are presented in Table 1. For Ni_2P and Co_2P-derived samples, it is noticed that the metal/phosphorus molar ratio was always higher than 1, which was the experimental ratio used for the metal phosphide incorporation process. This value is due to the partial elimination of phosphorus during the reduction process in the form of gaseous P_xH_y.[26,48] Using m-Al_2O_3 as support, the metal to phosphorus ratios are closer to the initial ratio used in the synthesis (1), suggesting that, although the formation of Ni and Co metallic phases takes place, instead of metal phosphides, a significant amount of phosphorus remain over the support surface.

The acidic properties of the Al-containing supports have been probed by ammonia TPD (see Fig. 4a). In the case of CMK-3, the NH_3-TPD analysis is not shown due to its lack of acidity. The TPD profiles indicate that Al-SBA-15 presents a moderate amount of acid sites with medium strength, as evidenced by the peak centered at around 270 °C, which corresponds with a NH_3 loss of 0.11 mmol/g. Mesoporous alumina exhibited a more intense and broader signal extending in the range 125 - 400 °C. The amount of ammonia desorbed in this case is considerable larger (about 0.46 mmol/g) than for Al-SBA-15, denoting that m-Al_2O_3 possesses a higher concentration of acid sites. However, the desorption peak for this last support is quite asymmetric and seems to be the result of at least two contributions, one at

Table 1 Physicochemical properties of both supports and passivated supported catalysts.

	S_{BET}[a] ($m^2\ g^{-1}$)	Total pore volume[b] ($cm^3\ g^{-1}$)	Pore diameter[c] (nm)	Impregnated nanoparticles size [d](nm)	Me/P molar ratio[e]
Al-SBA-15	869.60	1.180	10.90	-	67*
Ni_2P/Al-SBA-15	523.59	0.680	10.12	10 (8.4)	1.42
Co_2P/Al-SBA-15	391.16	0.640	10.12	8 (10.3)	1.22
MoP/Al-SBA-15	329.45	0.410	9.35	-	0.96
CMK-3	1145	1.178	2.97	-	-
Ni_2P/ CMK-3	792.60	0.487	2.93	9.2 (9.2)	1.55
Co_2P/ CMK-3	752.12	0.476	2.91	4.9**	1.31
MoP/ CMK-3	653.80	0.463	2.92	-	0.8
m-Al_2O_3	344.65	0.499	4.26	-	-
Ni_2P/m-Al_2O_3	165.89	0.229	4.87	7.5 (7.9)	1.34
Co_2P/m-Al_2O_3	153.10	0.209	4.25	9.5 (6.3)	1.02
MoP/m-Al_2O_3	206.10	0.267	4.28	-	0.52

[a]BET surface area from N_2 isotherm (77 K). [b]Total pore volume measured at P/P_0 = 0.97. [c]Pore diameter calculated applying BJH method to the adsorption branch. [d]Metal phosphide size from TEM images. Values within brackets were calculated from Scherrer's equation applied of the most intense diffraction peak. [e] Metal/Phosphorus molar ratio from ICP-AOS analysis. * Si/Al ratio from ICP- AOS analysis. **The signal of the most intense diffraction peak was inadequate to use the Scherrer's equation.

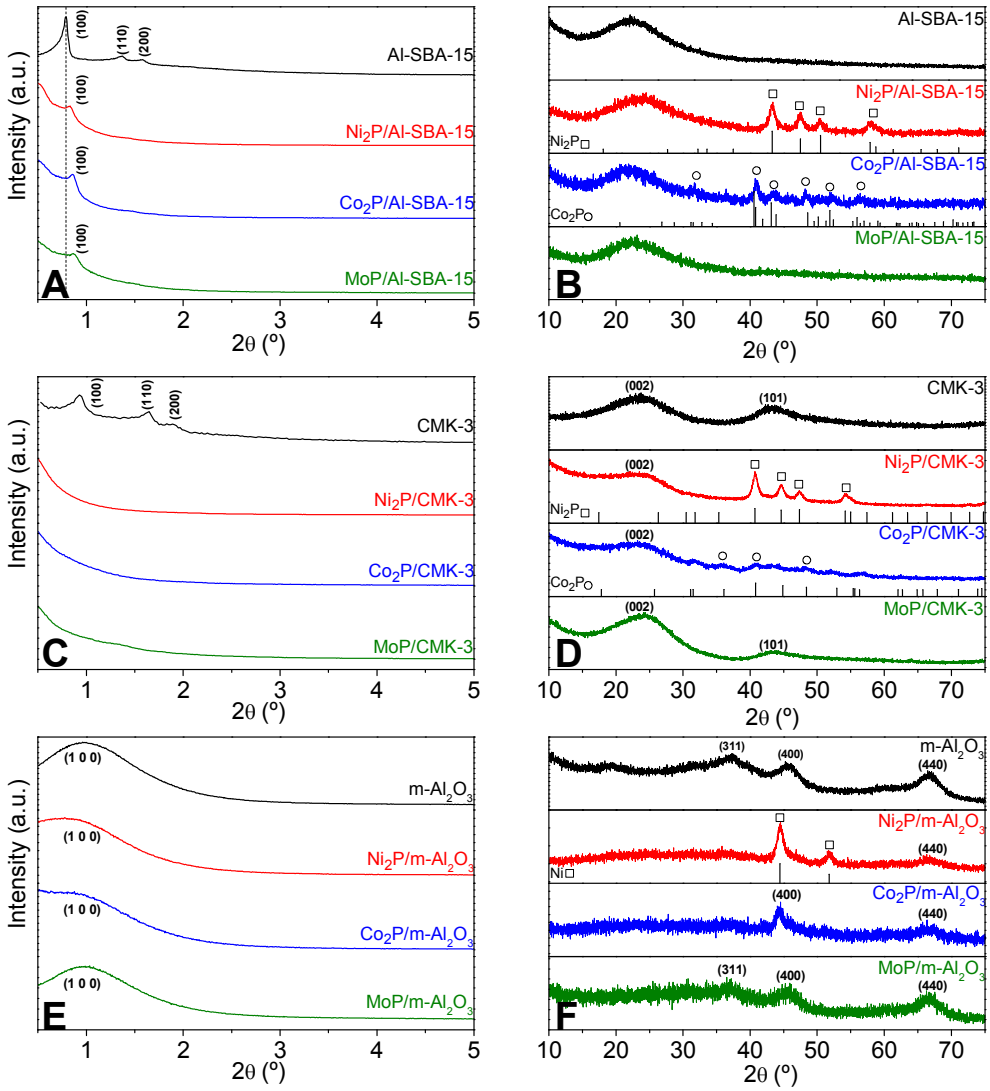

Fig. 2 X-ray diffraction patterns at low (A, C and E) and wide angle (B, D and F) for both supports and passivated supported catalysts.

about 180 °C and other located around 270 °C, which would correspond with acid sites of weak and medium strength, respectively. The high concentration of acid sites in m-Al_2O_3 may promote metal-support interactions, inhibiting the formation of the Ni and Co metal phosphides phases, as above observed in the XRD patterns.

In order to clarify the relationship between the incorporation of each metal phosphide and the overall acidity of the resulting material, the NH_3-TPD profiles corresponding to the catalysts prepared using Al-SBA-15 as support are drawn in Fig 4b. After the metal phosphide loading, a new peak appears at low temperatures, denoting the generation of weak acid sites. This effect is more pronounced in the case of Mo, followed by Ni and finally Co. Similar results have been earlier obtained by Chen et al.[27], being assigned to the Brönsted acidity generated by P-OH groups. In particular, for the Mo-containing sample, the sharp increase in the acidity is a clear indication of the presence of a high proportion of oxidized P species as a consequence of the low stability of the the MoP phase when exposed to air. In addition, it can be observed that the ammonia TPD curve of the Ni_2P/Al-SBA-15 sample shows a shoulder at medium-high temperature (between 250 and 450 °C), leading to enhanced ammonia desorption compared to the support. Interestingly, this fact is not observed for the Co_2P/Al-SBA-15 material, which indicates that the Ni phosphide phase presents some acidic features, which may affect its catalytic properties in HDO reactions, as further discussed.

Catalytic activity

Once the catalysts were reduced at 650 °C and passivated, they were tested in the phenol HDO reaction at 220 °C and 40 bar of pure hydrogen during 2 h. Both phenol conversion and HDO efficiency attained are presented in Fig. 5. Under the

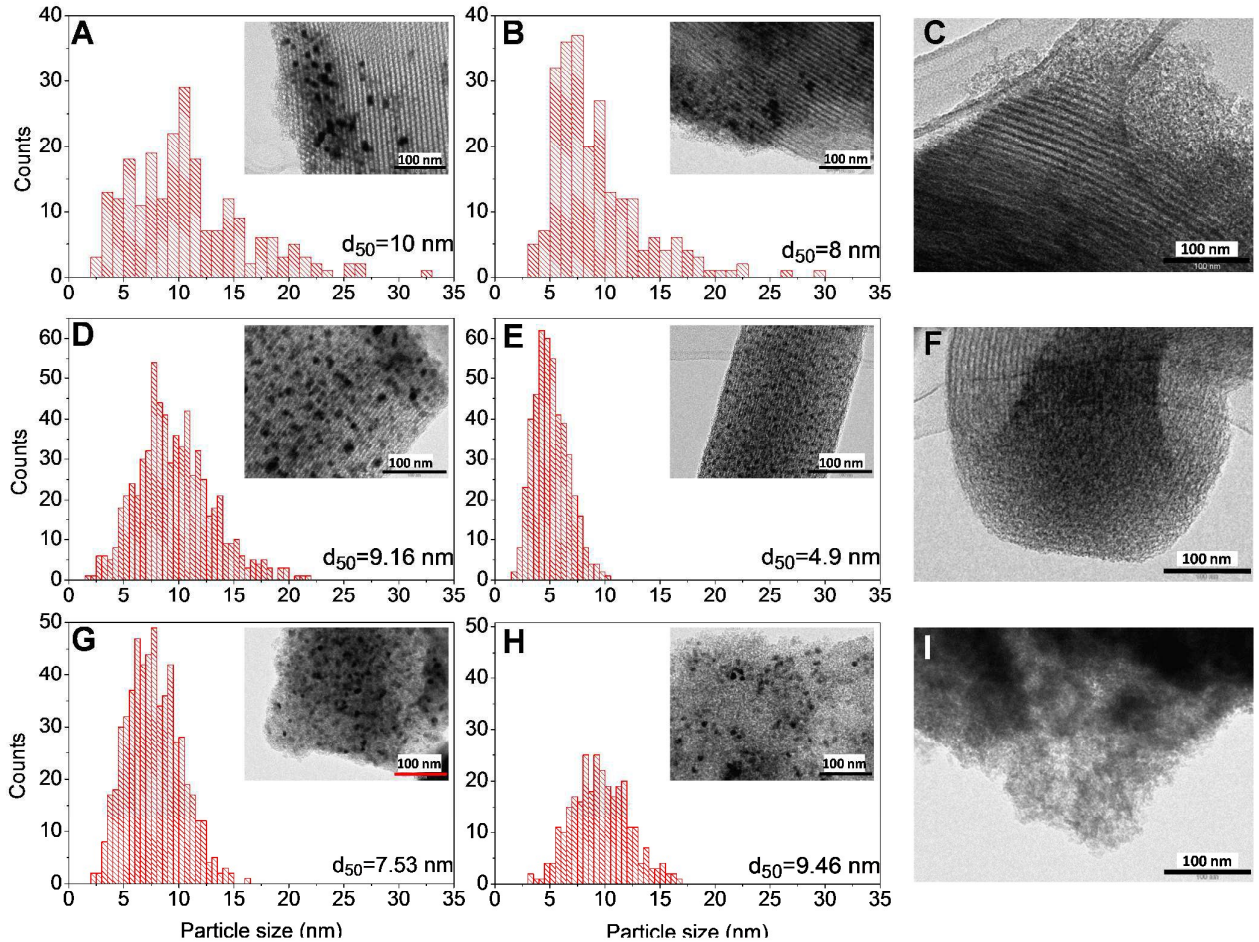

Fig. 3 TEM images and particle size distribution of passivated supported catalysts: (A) Ni_2P/Al-SBA-15, (B) Co_2P/Al-SBA-15, (C) MoP/Al-SBA-15, (D) Ni_2P/CMK-3, (E) Co_2P/CMK-3, (F) MoP/CMK-3, (G) Ni_2P/m-Al_2O_3, (H) Co_2P/m-Al_2O_3, (I) MoP m-Al_2O_3.

conditions employed, almost full conversion was obtained over Ni_2P/Al-SBA-15, Ni_2P/m-Al_2O_3 and Co_2P/m-Al_2O_3 catalysts, whereas Co_2P/Al-SBA-15 converted 82.9% of the initial phenol. The rest of catalysts led to much smaller conversions, below 50%. Comparing the same activity phase on different supports the use of ordered mesoporous carbon is clearly the less advantageous. The relatively low activity achieved with the carbonaceous support is attributed to its non-acidic nature, since acid sites have been found to strongly favour the HDO reactions over other substrates such as anisole.[49,50] On the other hand, molybdenum phosphide-based catalysts presented the worst activity, with negligible conversions when CMK-3 was used as support and reaching a maximum value of 21% over Al-SBA-15.

As an attempt to elucidate the reason of the activity differences between the active phases, H_2-TPR analysis of the catalysts prepared using Al-SBA-15 as support was performed. Fig. 6 shows the resultant H_2 consumption curves of each calcined catalyst before and after reduction treatments in the tubular furnace. Calcined Ni_2P/Al-SBA-15 shows a broad peak from 500 °C to more than 900 °C, attributed to an overlapping

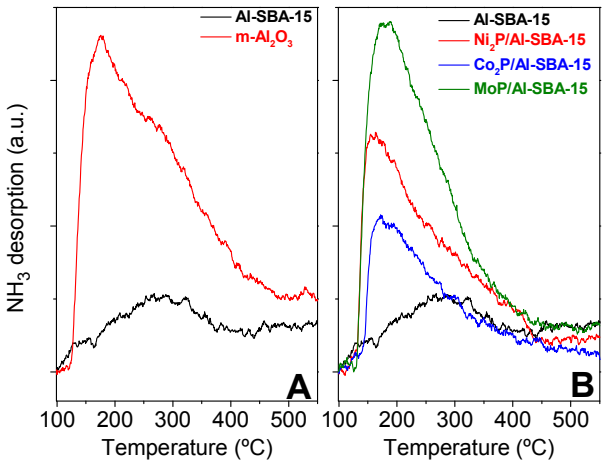

Fig. 4 NH_3-TPD profiles of Al-SBA-15, m-Al_2O_3 and passivated metal phosphides supported on Al-SBA-15.

in the reductions of both the nickel and phosphorous precursors, respectively.[27] When cobalt phosphide precursor was loaded into the support, a main peak at higher temperatures (890 °C) appeared. Despite this peak showed a shoulder denoting overlapping with reduction reactions at lower temperatures, it is much narrower than in the case of Ni_2P formation and reveals a higher interaction with the support. This result is in agreement with the smaller nanoparticle sizes and higher dispersion achieved for cobalt phosphide, as described before from TEM and XRD analysis. In both cases, the estimated hydrogen consumption for the catalysts reduction was similar (77.8 and 76.2 cm^3/g, respectively). In the case of calcined MoP/Al-SBA-15 catalyst, the behaviour was different comparing with the other two active phases: two peaks emerged indicating that the reduction of MoP precursor occurred in two steps. The first one, at lower temperature (maximum at 426 °C), is attributed to the reduction of MoO_3 to MoO_2 while the second one (centered at 652 °C) reveals the consecutive reduction of both molybdenum and phosphorus precursors to obtain MoP.[51]

After reduction treatment in a tubular furnace, the TPR patterns obtained were quite different in the case of both Ni_2P and Co_2P/Al-SBA-15 materials, with still significant hydrogen consumptions (24.04 and 12.52 cm^3/g, respectively) and revealing the coexistence of different species. Thus, Ni_2P/Al-SBA-15 presented four peaks along a wide range of temperatures: the first one appeared at 150 °C and it is attributed to the chemical reaction between hydrogen and Ni_2P. The next peak, at around 394 °C, is assigned to the reduction of a nickel oxide layer generated around the nickel phosphide particles during the passivation step with air. Finally, a broad signal at higher temperatures with two maximum H_2 consumptions (662 and 930 °C) are attributed to the reductions of nickel oxy-phosphates species and of P-O bonds, respectively. Similar interpretation, concerning the reduction of cobalt oxide layers and the existence of some unreacted metal and phosphorous precursors, can be done for the reduced Co_2P/Al-SBA-15 sample, which exhibited two peaks at around 416 and 760 °C. Therefore, the reduction treatment in the tubular furnace could not be totally efficient since a small part of the initial precursors seemed to be in their original form.

The most remarkable result was obtained in the case of reduced MoP/Al-SBA-15, since its TPR curve and total consumed hydrogen amount were quite similar to the same sample before the reduction treatment. These results, together with the difficulty to detect such active phase by either XRD or TEM analysis, suggested that MoP is highly unstable and with a high tendency to form the corresponding oxidized species. To get further inside in this idea, several H_2-TPR assays with an in-situ reduction treatment of the reduced sample have been done, the resultant curves being shown in Fig 7.

The first assay consisted in reducing in situ the catalyst (Fig. 7c) at the temperature of the HDO reaction tests (220 °C) and no differences with the previous TPR results (Fig. 7a and b)

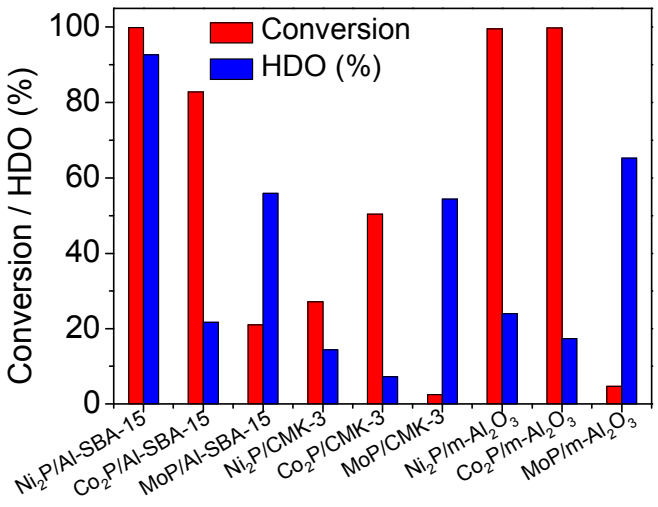

Fig. 5 Phenol conversion and HDO (%) over Ni, Co and Mo phosphides supported catalysts.

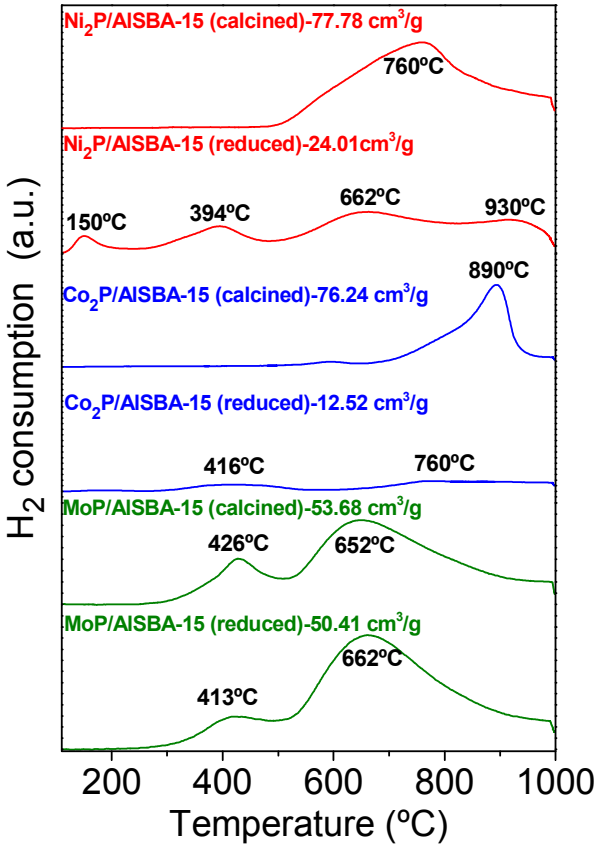

Fig. 6 TPR profiles of fresh (calcined) and passivated metal phosphides supported Al-SBA-15.

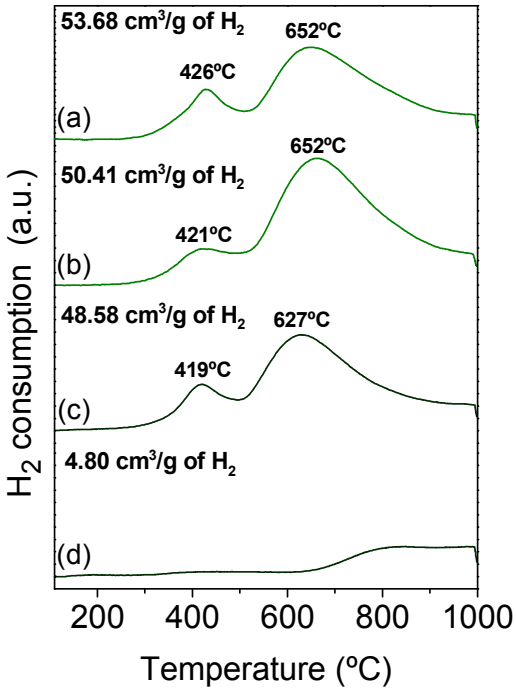

Fig. 7 TPR profiles of MoP/Al-SBA-15, (A) calcined, (B) passivated, (C) calcined and reduced in situ at 220°C and (D) calcined and reduced in situ at 650°C.

were detected. On the other hand, when the sample was subjected to an in-situ treatment with H_2 at 650 °C (Fig 7d), which is the reduction temperature in the tubular furnace; the H_2 consumption was very low. This result confirmed that the molybdenum phosphide phase is generated during the standard reduction treatment but is highly unstable in presence of air, being quickly re-oxidized and it explains the very low catalytic activity observed for their derived catalysts.

To get further insights about the formation of Mo phosphide phases during the reduction process, in situ XRD analyses using a high-temperature chamber under conditions similar to those employed in the reduction treatments have been performed. While during the heating ramp no new diffraction peak was observed (see SI Figure), when reaching a temperature of 600 °C, a broad low intensity peak appeared in the 33°-47° 2θ range. This signal remained unaltered during both the constant temperature step and the cooling of the sample provided that a H_2 atmosphere is kept. However, when air was passed through the chamber, after reaching a temperature of 30 °C, the broad XRD peak rapidly disappeared.

These results confirm that the Mo reduction takes place even at a relatively low temperature of 600 °C. The appearance of a broad XRD signal could be related with the formation of different types of highly dispersed Mo phosphide species. In this respect MoP, Mo_3P and MoP_2 phases present reflections in this interval, so it is not possible to determine the exact stoichiometry by this technique. Nevertheless, it can be concluded that the temperature program used in the reduction process in this work is enough to achieve the formation of Mo_xP_y species. Once H_2 is replaced by air, the peak generated during the reduction disappears even at room temperature, corroborating the high instability of Mo phosphide. This fact explains why these phases are not usually observed in the ex-situ XRD patterns of the samples.

Concerning the mechanisms by which phenol may undergo HDO reactions, previous investigations have demonstrated that there are two main parallel pathways.[4,6,48] a) direct hydrogenolysis of the C-O bond (DDO) leading to benzene as product and b) hydrogenation (HYD) involving a pre-hydrogenation of the aromatic ring to form cyclohexanol, followed by elimination of water and subsequent hydrogenation to form cyclohexane. However, from the GC analysis of the reaction products, additional compounds corresponding to addition or condensation reactions yielding molecules with two C6 rings were detected in minor amounts. Accordingly, Fig. 8 represents the proposed reaction pathways for the conversion of phenol under the experimental conditions employed in this work.

Fig 9 illustrates the distribution of products, in terms of selectivity, obtained for every catalyst tested. Strong differences can be observed, revealing the important influence of both the support nature and the type of metal phosphide loaded. The three catalysts based on Mo as precursor of the metal phosphide exhibit, not only low conversions, but also poor selectivity since the variety of compounds produced denoted the occurrence of two main reaction pathways: direct hydrogenolysis of the C-O bond (DDO) and hydrogenation (HYD). On the other hand, the major product of both Ni and Co phosphides supported on mesoporous carbon was found to be cyclohexanol (73.4 and 85.9% respectively), in addition to much lower amounts of cyclohexanone (11.8 and 6.9%) and cyclohexene (12.29 and 3.9%). These results suggest that the principal pathway of phenol reaction over both catalysts is the complete hydrogenation of the aromatic ring (HYD) following this route: phenol → cyclohexanone → cyclohexanol (Fig. 8).

Similarly to CMK-supports, when both Ni and Co were supported over m-Al_2O_3, the main product obtained was cyclohexanol (74 and 82%, respectively) and the second major product was cyclohexane (22.2 and 17%). However, there are three discrepancies denoting different reaction pathways: a) the conversion achieved was quite higher, close to 100%, b) benzene was negligible or even not detected and c) larger molecules formed by condensation reactions were detected in small amounts. The absence of benzene, denoting that direct deoxygenation route did not occur, together with the extremely high conversion of phenol was attributed to the formation of metallic Ni and Co species instead of their corresponding phosphides, as it was concluded from the XRD analyses. Besides, several studies have reported the strong interaction between Ni and Co with alumina and the weak Me-P interaction for metal phosphides in the same support.[52,53]

This strong interaction could promote the formation of mixed oxides with alumina, such as the $NiAl_2O_4$ or $CoAl_2O_4$ spinels, decreasing the acidity of the support and, therefore, limiting the deoxygenation capacity by reducing the availability of metallic sites.[52] Nevertheless, some acidic properties must be retained on the catalyst since small concentrations of large

molecules formed by condensation of two C6 rings have been observed, the condensation reactions being catalyzed by acidic sites.

In the case of Ni and Co phosphides supported on Al-SBA-15, phenol conversions were ~100% and 82.9%, respectively. For Ni_2P, the product distribution was different in comparison with the results obtained using CMK-3 and m-Al_2O_3 as supports: cyclohexane was the main product with 91% of selectivity. Since, according to Fig. 8, cyclohexane is the product corresponding to the complete hydrodeoxygenation reaction of phenol, this result evidences that this catalyst is very effective with high reaction rates of the intermediate steps. On the other hand, Co_2P/Al-SBA-15 showed higher selectivity to cyclohexanol (77.8 %) and, hence, lower HDO capacity. Due to the mild acidic nature of the support, minor amounts of larger ether molecules formed by condensation reactions were observed over both catalysts.

Both phenol conversion and product evolution was followed in more detail for the Ni_2P and Co_2P/Al-SBA-15 catalysts by carrying out reactions at shorter times (Fig. 10). In the former case, during the first hour of reaction, with phenol conversions below 60%, both cyclohexanol and cyclohexane were the most abundant products, while other intermediates appeared in much smaller amounts according to faster conversion rates. At longer times, phenol conversion rapidly increased and deoxygenation of cyclohexanol to yield cyclohexane was observed, so that at the end of the test the selectivity to cyclohexane was about 90%. According to this analysis, it was confirmed that hydrodeoxygenation of phenol over Ni_2P/Al-SBA-15 occurred preferentially through the HYD route, with minor contribution of direct hydrogenolysis pathway (DDO). In the case of Co_2P/Al-SBA-15, the overall reaction proceeded more slowly and the selectivity to cyclohexanol was much higher and stable during the progress of the reaction. Moreover, a limit on the phenol conversion at 80% seems to appear, which can be interpreted as a signal of catalyst deactivation.

In order to check the effect of the possible presence of metal oxide phases and metallic species when using the Al-SBA-15 support, two additional reactions were carried out using NiO/Al-SBA-15 and Ni^0/Al-SBA-15 as catalysts. In the case of NiO/Al-SBA-15 no phenol conversion was observed, confirming that the oxide has negligible activity in the HDO reaction. In contrast, when Ni^0/Al-SBA-15 was tested as a catalyst, phenol conversion was close to 100 %, similarly to that observed over Ni_2P/Al-SBA-15. However, great changes occurred in the products distribution. Thus, although cyclohexane was also the major product obtained over Ni^0/Al-

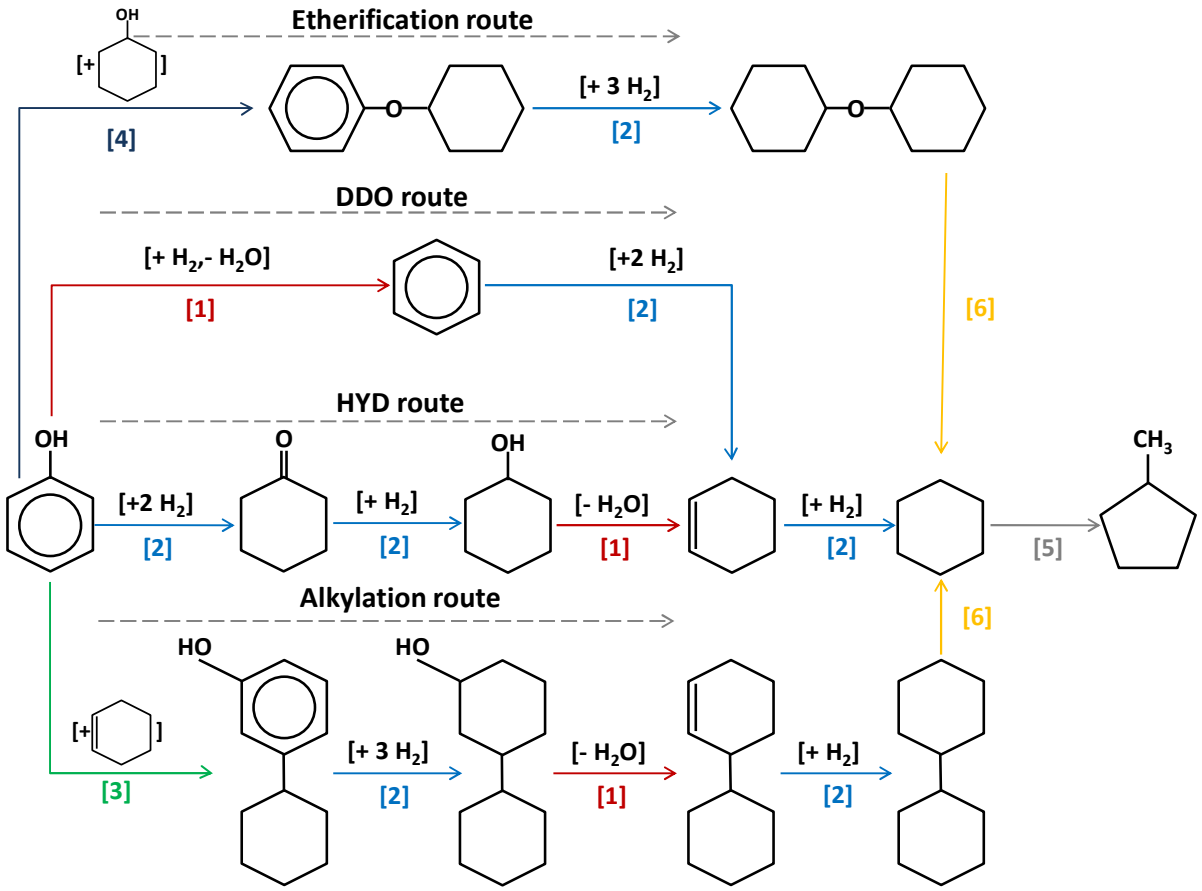

Fig. 8 Reaction network in phenol transformation 1) Hydrogenolysis, 2) Hydrogenation, 3) Alkylation, 4) Etherification, 5) Isomerization, 6) Dealkylation and detherification.

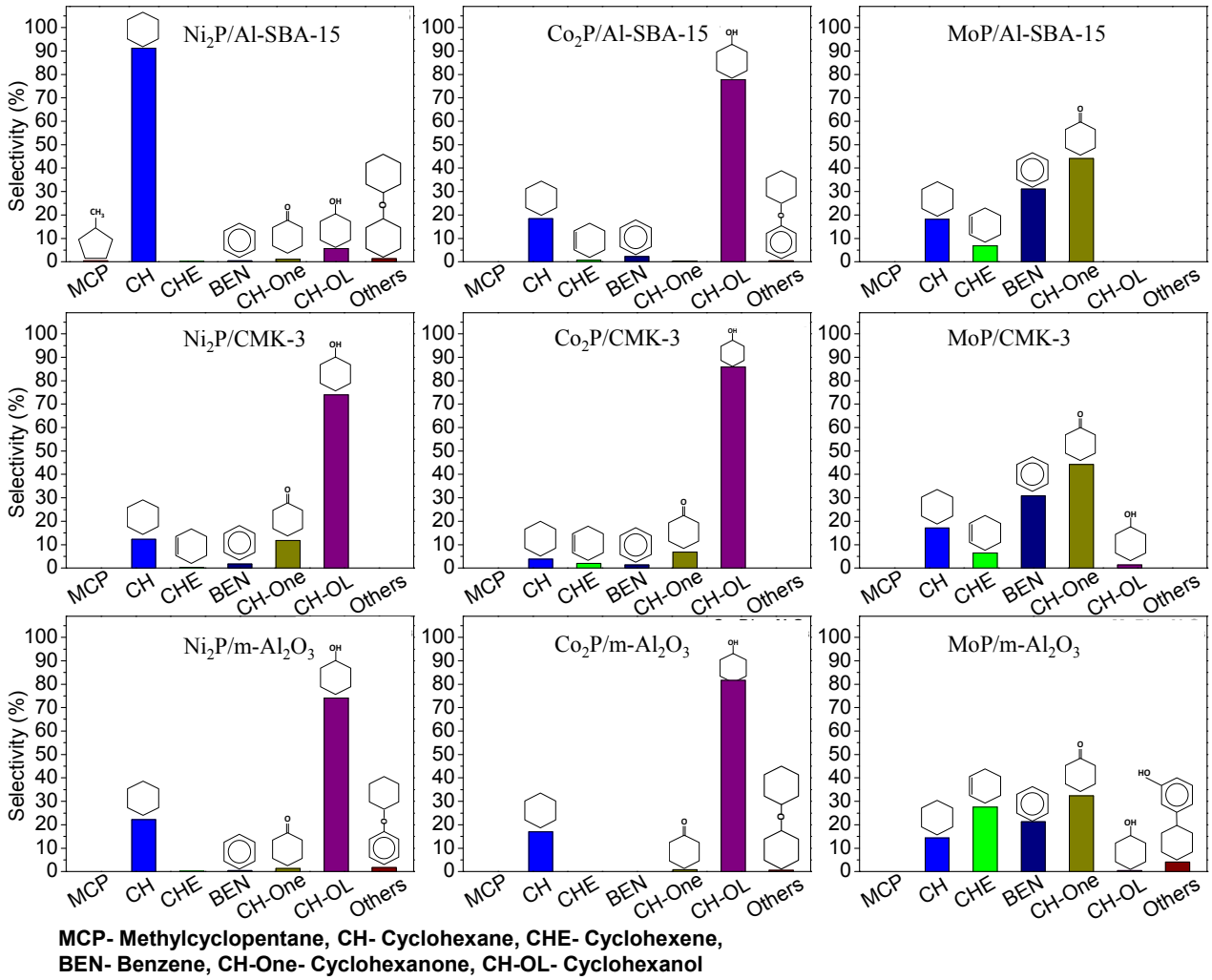

Fig. 9 Product distribution (%) reached over Ni, Co and Mo phosphides supported catalysts.

SBA-15, it was produced with a selectivity significantly lower than over Ni_2P/Al-SBA-15 (57.4 % and 91%, respectively)

Moreover, cyclohexanol was the second major product, with a selectivity of 41.8%, revealing that the presence of metallic Ni leads to the complete hydrogenation of the aromatic ring but with a lowered HDO efficiency.

Taking into account all the catalytic results previously described, it is clearly evidenced that Ni_2P/Al-SBA-15 is the only catalyst providing extremely high HDO efficiency exhibiting almost full phenol conversion together with cyclohexane selectivity higher than 90 %. This may be due to a synergetic effect between the high electron deficiency, generated by the $Ni^{\alpha+}$ ($0 < \alpha < 1$) species owing to an electron transfer from Ni to P, and the different acid sites present in the catalyst. As a result, Ni sites show enhanced capability for adsorbing and activating H_2, facilitating the hydrogen activation causing both HDO and aromatic ring saturation.[27,54] On the other hand, it is probable that the acidic features of this system, arising from both the Al-SBA-15 support and the nickel phosphide itself, enhance the interaction with the phenol molecules, causing their adsorption and favouring their subsequent transformation through aromatic ring hydrogenation and HDO reactions.

Conclusions

The synthesis of Ni_2P, Co_2P and MoP over three supports presenting different physicochemical properties (mesoporous acidic ɣ-Al_2O_3; ordered mesoporous acidic aluminosilicate, Al-SBA-15, and ordered mesoporous carbon, CMK-3) has been investigated. The physicochemical analysis indicated that both the dispersion and metal phases attained are strongly influenced by the support nature and, in particular, its acidity. The dispersion of metal derived nanoparticles over the supports increases in the following order: Al-SBA-15 < m-Al_2O_3 < CMK-3. From XRD, TEM and H_2-TPR results, it was revealed that MoP phase is probably formed but very rapidly re-oxidized in presence of air. On the other hand, metal

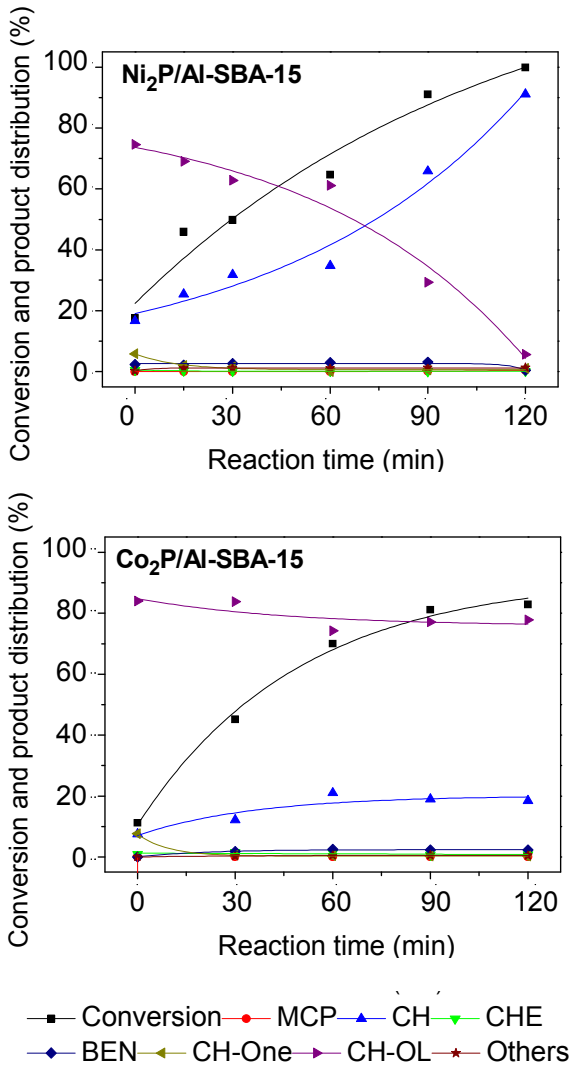

Fig 10 Phenol conversion and product distribution (%) at different times of reaction.

phosphide formation was hindered over m-Al_2O_3 as only metallic Ni and Co were detected.

All the materials prepared have been evaluated as potential catalysts in hydrodeoxygenation (HDO) reaction for upgrading pyrolysis bio-oils. Reactions tests have been carried out using phenol as bio-oil model compound. It has been denoted the importance of an appropriate selection of the support since the highest phenol conversions were attained with the acidic ones (Al-SBA-15 and m-Al_2O_3). The type of metal phosphide, as well as the role of the support on the formation and dispersion of such active phases, evidenced by the characterization techniques, has a significant effect on the HDO efficiency. Thus, despite the high conversions, Co_2P/Al-SBA-15, Ni_2P/m-Al_2O_3 and Co_2P/m-Al_2O_3 yielded cyclohexanol as main product denoting very low HDO performance.

Ni_2P/Al-SBA-15 is the only catalyst providing extremely high HDO efficiency, exhibiting almost full phenol conversion together with cyclohexane selectivity higher than 90 %. This remarkable behaviour can be assigned to a synergetic effect between the high electron deficiency, generated by the $Ni^{\alpha+}$ ($0 < \alpha < 1$) species owing to an electron transfer from Ni to P, and the different acid sites present in the catalyst.

Acknowledgements

This work has been supported by the Spanish Ministry of Economy and Competitiveness though LIGCATUP project (ENE2011-29643-C02-01), the European Union Seventh Framework Programme (FP7/ 2007-2013) under grant agreement n°604307 (CASCATBEL project) and by the regional government of Madrid through RESTOENE research project (Ref: P2009/ENE-1743, Consejería de Educación de la Comunidad de Madrid).

Notes and references

1 G. W. Huber, S. Iborra and A. Corma, *Chem. Rev*, 2006, **106**, 4044–98.
2 D. C. Elliott, *Energ. Fuel.*, 2007, **21**, 1792–1815.
3 D. E. Resasco, *J. Phys. Chem. Lett.*, 2011, **2**, 2294–2295.
4 T. N. Pham, D. Shi and D. E. Resasco, *Appl. Catal. B-Environ.*, 2014, **145**, 10–23.
5 Z. He and X. Wang, *Catal. Sustainable Energy*, 2012, **1**, 28–52.
6 E. Furimsky, *Appl. Catal. A-Gen.*, 2000, **199**, 147–190.
7 P. M. Mortensen, J.-D. Grunwaldt, P. A. Jensen, K. G. Knudsen and A. D. Jensen, *Appl. Catal. A-Gen.*, 2011, **407**, 1–19.
8 A. Y. Bunch, X. Wang and U. S. Ozkan, *J. Mol. Catal. A-Chem.*, 2007, **270**, 264–272.
9 M. Badawi, J. F. Paul, S. Cristol, E. Payen, Y. Romero, F. Richard, S. Brunet, D. Lambert, X. Portier, A. Popov, E. Kondratieva, J. M. Goupil, J. El Fallah, J. P. Gilson, L. Mariey, A. Travert and F. Maugé, *J. Catal.*, 2011, **282**, 155–164.
10 J. Horáček, F. Homola, I. Kubičková and D. Kubička, *Catal. Today*, 2012, **179**, 191–198.
11 O. İ. Şenol, E.-M. Ryymin, T.-R. Viljava and A. O. I. Krause, *J. Mol. Catal. A-Chem.*, 2007, **277**, 107–112.
12 E. Laurent and B. Delmon, *Appl. Catal. A-Gen.*, 1994, **109**, 97–115.
13 M. Ferrari, S. Bosmans, R. Maggi, B. Delmon and P. Grange, *Catal. Today*, 2001, **65**, 257–264.
14 G. de la Puente, A. Gil, J. J. Pis and P. Grange, *Langmuir*, 1999, **15**, 5800–5806.
15 V. N. Bui, D. Laurenti, P. Delichère and C. Geantet, *Appl. Catal. B-Environ.*, 2011, **101**, 246–255.
16 J. Ramirez, S. Fuentes, G. Díaz, M. Vrinat, M. Breysse and M. Lacroix, *Appl. Catal.*, 1989, **52**, 211–224.
17 A. Gutierrez, R. K. Kaila, M. L. Honkela, R. Slioor and A. O. I. Krause, *Catal. Today*, 2009, **147**, 239–246.
18 J. Wildschut, I. Melián-Cabrera and H. J. Heeres, *Appl. Catal. B-Environ.*, 2010, **99**, 298–306.
19 X. Zhu, L. L. Lobban, R. G. Mallinson and D. E. Resasco, *J. Catal.*, 2011, **281**, 21–29.
20 B. Dhandapani, T. S. Clair and S. T. Oyama, *Appl. Catal. A-Gen.*, 1998, **168**, 219–228.
21 E. Furimsky, *Appl. Catal. A-Gen.*, 2003, **240**, 1–28.
22 W. Zhang, Y. Zhang, L. Zhao and W. Wei, *Energ. Fuel.*, 2010, **24**, 2052–2059.
23 T. Prasomsri, T. Nimmanwudipong and Y. Román-Leshkov, *Energ. Environ. Sci.*, 2013, **6**, 1732–1738.

24 V. M. L. Whiffen and K. J. Smith, *Energ. Fuel*., 2010, **24**, 4728–4737.
25 D. R. Moberg, T. J. Thibodeau, F. G. Amar and B. G. Frederick, *J. Phys. Chem. C*, 2010, **114**, 13782–13795.
26 S. T. Oyama, T. Gott, H. Zhao and Y.-K. Lee, *Catal. Today*, 2009, **143**, 94–107.
27 J. Chen, H. Shi, L. Li and K. Li, *Appl. Catal. B-Environ*., 2014, **144**, 870–884.
28 T. Koranyi, Z. Vit, D. Poduval, R. Ryoo, H. Kim and E. Hensen, *J. Catal*., 2008, **253**, 119–131.
29 Y.-K. Lee and S. T. Oyama, *J. Catal*., 2006, **239**, 376–389.
30 S. T. Oyama, X. Wang, Y.-K. Lee, K. Bando and F. G. Requejo, *J. Catal*., 2002, **210**, 207–217.
31 S. Boullosa-Eiras, R. Lødeng, H. Bergem, M. Stöcker, L. Hannevold and E. A. Blekkan, *Catal. Today*, 2014, **223**, 44–53.
32 H. Y. Zhao, D. Li, P. Bui and S. T. Oyama, *Appl. Catal. A-Gen*., 2011, **391**, 305–310.
33 P. Bui, J. A. Cecilia, S. T. Oyama, A. Takagaki, A. Infantes-Molina, H. Zhao, D. Li, E. Rodríguez-Castellón and A. Jiménez López, *J. Catal*., 2012, **294**, 184–198.
34 Y. Yang, C. Ochoa-Hernández, V. A. de la Peña O'Shea, P. Pizarro, J. M. Coronado and D. P. Serrano, *Appl. Catal. B-Environ*., 2014, **145**, 91–100.
35 R. Prins and M. E. Bussell, *Catal. Lett*., 2012, **142**, 1413–1436.
36 A. Rodriguez, J. Kim, J. C. Hanson, S. J. Sawhill and M. E. Bussell, *J. Phys. Chem. B*, 2003, **107**, 6276–6285.
37 Y. Yang, J. Chen and H. Shi, *Energ. Fuel.,* 2013, **27**, 3400–3409.
38 Q. Bu, H. Lei, A. H. Zacher, L. Wang, S. Ren, J. Liang, Y. Wei, Y. Liu, J. Tang, Q. Zhang and R. Ruan, *Bioresource Technol*., 2012, **124**, 470–477.
39 Y. Yue, A. Gédéon, J.-L. Bonardet, J.-B. D'Espinose, J. Fraissard and N. Melosh, *Chem. Commun*., 1999, **19**, 1967–1968.
40 J. Aguado, J. M. Escola, M. C. Castro and B. Paredes, *Micropor. Mesopor. Mat*., 2005, **83**, 181–192.
41 P. A. Bazuła, A.-H. Lu, J.-J. Nitz and F. Schüth, *Micropor. Mesopor. Mat*., 2008, **108**, 266–275.
42 D. P. Serrano, J. A. Botas, P. Pizarro, R. Guil-López and G. Gómez, *Chem. Commun*., 2008, **48**, 6585–6587.
43 D. Zhao, P. Yang, Q. Huo, B. F. Chmelka and G. D. Stucky, *Curr. Opin. Solid St. M*., 1998, **3**, 111–121.
44 D. Zhao, J. Feng, Q. Huo, N. Melosh, G. Fredrickson, B. Chmelka and G. Stucky, *Science*, 1998, **279**, 548–52.
45 Y. Yang, C. Ochoa-Hernández, P. Pizarro, V. A. de la Peña O'Shea, J. M. Coronado and D. P. Serrano, *Top. Catal.*, 2012, **55**, 991–998.
46 J. M. R. Gallo, C. Bisio, G. Gatti, L. Marchese and H. O. Pastore, *Langmuir*, 2010, **26**, 5791–800.
47 N. Lin, J. Y. Yang, Z. Y. Wu, H. J. Wang and J. H. Zhu, *Micropor. Mesopor. Mat.*, 2011, **139**, 130–137.
48 J. Chen, Y. Chen, Q. Yang, K. Li and C. Yao, *Catal. Commun*., 2010, **11**, 571–575.
49 S. Jin, Z. Xiao, C. Li, X. Chen, L. Wang, J. Xing, W. Li and C. Liang, *Catal. Today*, 2014, **234**, 125–132.
50 T. M. Sankaranarayanan, A. Berenguer, C. Ochoa-Hernández, I. Moreno, P. Jana, J. M. Coronado, D. P. Serrano and P. Pizarro, *Catal. Today*, 2014, **243**, 1–10.
51 A. Montesinos-Castellanos, T. A. Zepeda, B. Pawelec, E. Lima, J. L. G. Fierro, A. Olivas and J. A. de los Reyes H., *Appl. Catal. A-Gen*., 2008, **334**, 330–338.
52 P. M. Mortensen, J. Grunwaldt, P. A. Jensen and A. D. Jensen, *ACS Catal*., 2013, **3**, 1774–1785.
53 S.-K. Wu, P.-C. Lai, Y.-C. Lin, H.-P. Wan, H.-T. Lee and Y.-H. Chang, *ACS Sustainable Chem. Eng*., 2013, **1**, 349–358.
54 E. Furimsky, *Catal. Today*, 2013, **217**, 13–56.

A series of transition metal phosphides (Ni_2P, Co_2P and MoP) supported over three mesoporous materials: Al-SBA-15, m-Al_2O_3 and CMK-3 have been probed as potential catalysts in hydrodeoxygenation (HDO) for upgrading pyrolysis bio-oils using phenol as bio-oil model compound.